Evolution of damping in ferromagnetic/nonmagnetic thin film bilayers as a function of nonmagnetic layer thickness

S. Azzawi,[1] A. Ganguly,[2] M. Tokaç,[1] R. M. Rowan-Robinson,[1] J. Sinha,[2] A. T. Hindmarch,[1] A. Barman,[2,*] and D. Atkinson[1,†]

[1]*Centre for Materials Physics, Durham University, South Road, Durham DH1 3LE, United Kingdom*
[2]*Department of Condensed Matter Physics and Material Sciences, S. N. Bose National Centre for Basic Sciences, India*

The evolution of damping in Co/Pt, Co/Au, and $Ni_{81}Fe_{19}$/Pt bilayers was studied with increasing nonmagnetic (NM) heavy-metal layer thicknesses in the range 0.2 nm $\leqslant t_{NM} \leqslant$ 10 nm, where t_{NM} is the NM layer thickness. Magnetization precession was measured in the time domain using time-resolved magneto-optical Kerr effect magnetometry. Fitting of the data with a damped sinusoidal function was undertaken in order to extract the phenomenological Gilbert damping coefficient α. For Pt-capped Co and $Ni_{81}Fe_{19}$ layers a large and complex dependence of α on the Pt layer thickness was observed, while for Au capping no significant dependence was observed. It is suggested that this difference is related to the different localized spin-orbit interaction related to intermixing and to d-d hybridization of Pt and Au at the interface with Co or $Ni_{81}Fe_{19}$. Also it was shown that damping is affected by the crystal structure differences in FM thin films and at the interface, which can modify the spin-diffusion length and the effective spin-mixing conductance. In addition to the intrinsic damping an extrinsic contribution plays an important role in the enhancement of damping when the Pt capping layer is discontinuous. The dependence of damping on the nonmagnetic layer thickness is complex but shows qualitative agreement with recent theoretical predictions.

I. INTRODUCTION

Precessional magnetization dynamics are fundamental to magnetic field and current-driven magnetization processes and underpin switching behavior in applications such as magnetic data storage, where data writing depends on the magnetic damping. Precessional damping plays an important role in a number of emerging technologies, including magnonics and spin transfer torque magnetoresistive random access memory (STT-MRAM) devices. Understanding and controlling damping in thin film systems therefore continues to drive research in this field. It has been demonstrated that damping can be enhanced in both bulk ferromagnetic (FM) [1–4] and multilayered systems [5–8] and many studies have addressed the fundamental origin of damping both experimentally and theoretically [1,3,9–15]. Both Co and $Ni_{81}Fe_{19}$ have attracted a lot of attention due to their common application in magnetic devices. More recently, the influence of heavy-metal (NM) overlayers on the damping in adjacent ferromagnetic (FM) layers has attracted a lot of research interest. In such bilayer systems there are several mechanisms that may lead to the enhancement of damping. Spin-orbit coupling (SOC) and interfacial d-d hybridization enhance the intrinsic damping, while extrinsic enhancement of the damping can arise from two-magnon scattering processes, linked to roughness and defects at the interface region [1–3,11–21]. The total precessional damping is a sum of the intrinsic and extrinsic contributions.

In the case of bilayer and multilayer thin films, the strong SOC of the heavy metal layer leads to enhanced damping because of enhanced coupling of the electron spin with the lattice at the interface. This will facilitate the propagation and dissipation of transverse spin current generated by precession in the ferromagnetic layer. NM layers can therefore act as an absorber or sink for spin current pumped across the interface [3,14]. The spin-current pumped into the adjacent NM layer may either dissipate in the NM layer or diffuse back into the FM layer. This depends on the spin diffusion length (λ_{sd}) and the effective spin-mixing conductance ($g_{\uparrow\downarrow}^{eff}$) across the interface [8]. The d-d electron hybridization of the FM/NM layer occurs at the interface and is therefore influenced by topological roughness and intermixing. These factors may also increase the local density of states at the Fermi energy or decrease the bandwidth in the interface region [3,11,13,17,21]. The specific electronic behavior depends on the materials involved and the damping has been studied in variety of systems, including Au, MgO, Cu, and Ta NM overlayers on FM layers of Co, CoFeB, and $Ni_{80}Fe_{20}$ [3,8,16,22].

Moving on to extrinsic damping contributions, two-magnon scattering refers to the scattering of uniform magnetization precession into pairs of magnons with nonzero wave vectors [3,16,22]. This can occur when the symmetry of the system is disturbed by structural defects like film roughness and intermixing [1,3,21] and will enhance the effective damping of the magnetization precession. Increased intermixing will also enhance the effective spin-mixing conductance [8,21,22], and modifying the interface will affect all of the mechanisms mentioned above [4,23]. It is therefore of great interest to study the evolution of precessional magnetic damping in FM/NM bilayers as the interface develops as a function of the NM thickness.

A recent theoretical study of FM/NM bilayers by Barati *et al.* [3] reported the dependence of damping with increasing thickness of the nonmagnetic layer, assuming an ideal flat interface. This predicted that for NM layers the damping depends on the specific material and the layer thickness.

───────────
*abarman@bose.res.in
†del.atkinson@durham.ac.uk

In particular, for the case of Co/Pt bilayers the magnetic damping was found to increase by more than two times with the addition of a few monolayers of Pt. This theoretical analysis motivates the experimental study of precessional damping as a function of NM capping layer thickness in this work. The experimental study requires well-controlled thin film deposition and also structural analysis in order to establish precise layer thicknesses, interface width, and FM crystal structure.

II. FORMALISM FOR ANALYSIS OF DAMPING

The measured effective magnetic damping α_{eff} can be written as the sum of the bulk, intrinsic and extrinsic contributions,

$$\alpha_{eff} = \alpha_0^{int} + \alpha_{ext}, \tag{1}$$

where α_0^{int} and α_{ext} are the total intrinsic and extrinsic damping coefficients of the system, respectively. Furthermore, α_0^{int} can be expressed such that

$$\alpha_{eff} = \frac{G_0}{\gamma M_s} + \alpha_s / t_{FM} + \alpha_{ext}, \tag{2}$$

where G_0 is the bulk Gilbert damping parameter, γ is the gyromagnetic ratio, M_s is the saturation magnetization, t_{FM} is the ferromagnetic layer thickness, and α_s is the interface contribution to the effective damping [3,12,24].

The thickness dependence of the damping enhancement may be explained by a mixture of spin-pumping, $d - d$ hybridization, and two-magnon scattering effects. In this study α_{eff} was measured as a function of the NM layer thickness.

III. EXPERIMENTAL DETAILS

The common and widely utilized ferromagnetic materials Co and $Ni_{81}Fe_{19}$ were studied with NM capping layers of Pt and Au. Bilayer thin films were deposited by UHV magnetron sputtering from a base pressure $\sim 10^{-8}$ torr on to thermally oxidized silicon substrate with a 100-nm SiO_2 layer. The complete structure was $Si/SiO_2/FM/NM$ and the FM layer was deposited directly on the SiO_2. The selected Co layer thicknesses were either 4 or 10 nm and for the $Ni_{81}Fe_{19}$ films the thickness was 7 nm. The thicknesses were chosen to maximize the interaction between the films and the incident optical probe. The thinnest capping layers may permit partial oxidation of the FM surface, but adding a further capping layer would make the physical system more complex, which could confuse the results. The study aimed to examine the subnanometer thickness effect of specific NM materials on the damping. Capping layer thicknesses were varied from 0.2 to 10 nm. Dynamic magnetization behavior was studied *ex situ* using time-resolved magneto-optical Kerr effect (TRMOKE) magnetometry using an all-optical pump-probe technique. More details about the TRMOKE system can be found elsewhere [25–27]. Structural analysis was carried out using a Bede-D1 diffractometer with a CuKα source for grazing incidence x-ray reflectivity (XRR) to study layer thicknesses and interfacial structure and for x-ray diffraction (XRD) to analyze crystal structure; more information can be found elsewhere [28,29]. True specular XRR data were obtained
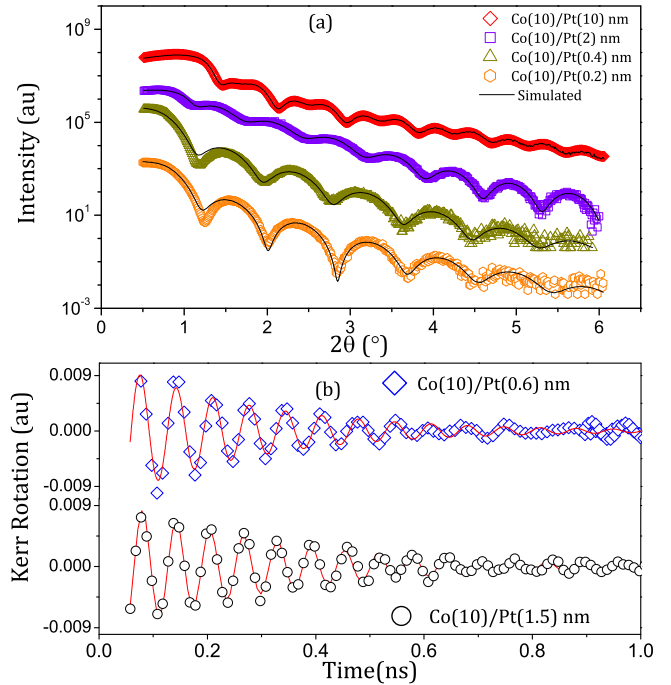

FIG. 1. (a) Examples of x-ray reflectivity data and the best-fitting simulations for Co (10 nm)/Pt (t_{Pt}). (b) Background subtracted time-resolved magneto-optic Kerr rotation data for Co/Pt with two different Pt layer thicknesses and the best-fitting damped sinusoids.

by subtraction of the measured forward diffuse scatter and was modeled with simulations generated using the GenX code, which uses a differential evolution algorithm with the Parrat recursive mechanism to simulate the XRR data [30]. XRD results were analyzed to determine the out-of-plane lattice parameter.

IV. RESULTS

Figure 1(a) shows examples of the XRR data obtained from selected samples and the corresponding best-fitting simulations. From the numerical analysis structural parameters were derived, including the layer thicknesses and interface roughness. Table I shows the thickness and roughness of selected FM/NM bilayers. These data were selected because they indicate the width of the FM/NM interfacial region when the NM metal forms a complete layer over the FM layer. The interface width includes topological roughness and intermixing. The interface width is important as it provides

TABLE I. Structural properties for selected Co/Au, Co/Pt, and NiFe/Pt bilayers samples extracted from XRR measurements: FM layer thickness, t_{FM}; NM layer thickness, t_{NM}; and interface width at FM/NM interface.

Sample structure	t_{FM} (nm)	t_{NM} (nm)	Interface width (nm)
Co (10 nm)/Au (4 nm)	9.44 ± 0.05	3.5 ± 0.04	0.61 ± 0.11
Co (10 nm)/Pt (2 nm)	9.56 ± 0.09	2.8 ± 0.05	0.66 ± 0.07
$Ni_{81}Fe_{19}$ (7 nm)/Pt (1 nm)	7.24 ± 0.11	0.94 ± 0.08	0.92 ± 0.05

an indication of the thickness at which the NM capping layer changes from islandlike coverage to continuous coverage of the FM layer. The structural analysis shows that both Pt and Au form a continuous layer on Co at a thickness greater than ~0.7 nm, while for $Ni_{81}Fe_{19}$ the NM capping layer becomes continuous at a thicknesses above ~0.9 nm. This difference in roughness between the two FM materials may stem from the crystal structure, which XRD shows is fcc for the $Ni_{81}Fe_{19}$ and hcp for the Co [3,15,22]. The Au and the Pt are both fcc. For Au and Pt capping of Co, the interfacial roughness is very similar; however, details of the local atomic arrangement are likely to differ, Co and Pt are miscible while Co and Au are immiscible [31]. The growth of Au or Pt capping layers onto a FM thin film layer begins with the formation of localized islands of the NM material; these expand and develop into a continuous capping layer as the NM thickness increases.

Figure 1(b) shows typical TRMOKE data for selected samples following removal of the ultrafast demagnetization and subtraction of a background signal by fitting with a biexponential function. The background signal represents the initial recovery of magnetization following an optically induced demagnetization and is characterized by two relaxation times of the order of 1 and 20 ps. The shorter time scale is related to electronic thermal bath dissipation to the lattice. The longer time scale is associated with dissipation of energy between the lattice and surroundings, which decreases with the addition of the capping layer. Returning to the figure, the TRMOKE data illustrate the magnetic precession, which show that FM-NM bilayers with certain NM capping thickness are damped faster. The figure also shows the best-fitting curves, which indicate a single-mode damped precession behavior representing the Landau-Lifshitz-Gilbert relation from which the damping coefficient was obtained.

Figures 2(a) and 2(c) show the variation of α_{eff} with Pt and Au layer thickness. It shows that α_{eff} increases significantly for both Co/Pt and $Ni_{81}Fe_{19}$/Pt layers as the Pt capping layer thickness increases and peaks around 0.7–0.8 nm for Co/Pt and 0.6 nm for $Ni_{81}Fe_{19}$/Pt. However, in the case of Co/Au, α_{eff} is nearly constant across the entire Au thickness range. Also, it should be noted that the bulk damping coefficient for hcp Co is 0.011; however, here the uncapped or the partially capped Co and $Ni_{81}Fe_{19}$ are likely to be partially oxidized and this may enhance α_{eff} from the bulk value. The interfacial width shown inTable I for $Ni_{81}Fe_{19}$/Pt may explain the increase in α_{eff} up to a capping layer thickness of 0.6 nm, but the available damping data is limited to thicknesses up to 1 nm.

The thickness dependence of the capping layer on α_{eff} for Co/Pt and $Ni_{81}Fe_{19}$/Pt may be divided into three different regions. With initial increasing Pt thickness the damping first increases rapidly (region I) and then peaks (region II) before falling back to a lower constant level (region III). These different regions are discussed in more detail later. Figure 2(b) shows the precessional frequency, f, and the saturation magnetization, M_S, as a function of NM layer thickness for the Co/Pt bilayer. A noticeable similarity of the Pt thickness dependence between M_S and f is observed. In particular, both M_S and f increase rapidly with Pt thickness between 0.6 and 0.8 nm.

In order to understand the damping mechanisms further a series of TRMOKE measurements were undertaken at
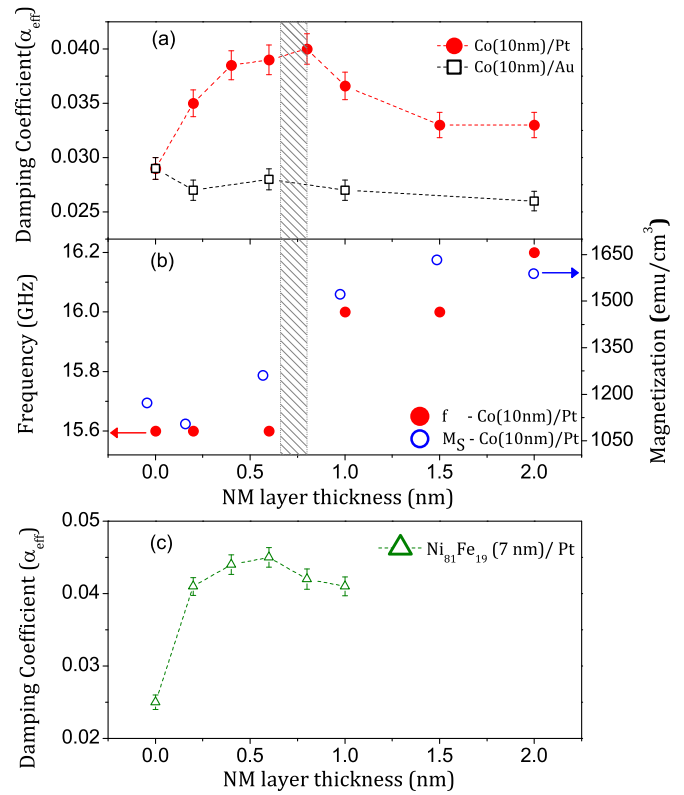

FIG. 2. [(a) and (c)] α_{eff} as a function of t_{NM} for Co/Pt and $Ni_{81}Fe_{19}$/Pt, respectively. (b) Frequency and saturation magnetization as a function of t_{NM} and ~1.4 kOe of magnetic field strength; it shows a similar trend in their variations. The shaded bar indicate the Pt thickness where the Pt became continuous.

different bias fields in order to look for a dependence on the precessional frequency, which can inform on the nature of the damping. Figure 3 shows examples of plots of α_{eff} as a function
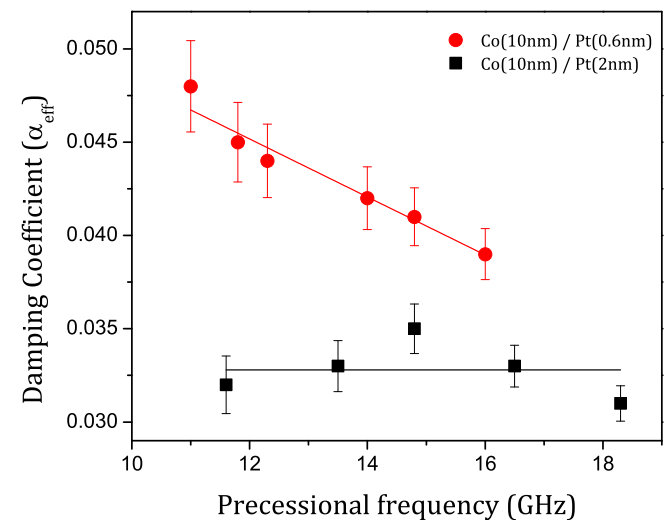

FIG. 3. Damping coefficient α_{eff} as a function of precessional frequency for 10-nm Co films capped with 0.6-nm and 2-nm Pt. The extrinsic damping decreases with the increasing Pt thickness until it reaches to negligible extrinsic effect at $t_{NM} = 2$ nm.

of f for a discontinuous (0.6 nm) and continuous (2 nm) Pt capping layer on Co. In the case of the discontinuous Pt layer the damping falls linearly with the increase in precessional frequency, while the damping remains almost constant with frequency for the continuous Pt-capped Co bilayer. For a continuous Pt capping layer on $Ni_{81}Fe_{19}$ the damping is also constant as a function of precessional frequency.

V. DISCUSSION

The complex dependence of α_{eff} with NM layer thickness described in Figs. 2(a) and 2(c) with three characteristic regions can be understood by considering several intrinsic and extrinsic effects occurring at the interface of the FM and NM layers. It is known that d-d hybridization, spin-pumping, and two-magnon scattering are the effective factors for damping enhancement in FM/NM thin films [3,4,11,13,17,21,23]. The experimental results are in agreement with a recent theoretical study [3] where damping increases with increasing Pt capping layer thickness up to a broad peak followed by a decrease to constant value with further increases in thickness. In the experimental work the Co structure is hcp, but fcc in the theoretical; however, a key point is that Pt and Au have fcc structure, which allows direct comparison [32].

The possible intrinsic contributions to enhancement of the damping in region I can be attributed to d-d hybridization and spin-pumping in the case of the Pt capping layer. Hybridization causes changes in the electronic structure in the interface, whereas spin-pumping allows absorption of angular momentum from the precessing magnetization, giving rise to an enhancement of damping. Both effects are intrinsic in nature.

However, the effect of spin pumping should be very limited over the studied thickness range of Pt, as it is comparable or below the spin-diffusion length, λ_{sd} [12,33–36]. Hence, d-d hybridization mainly contributes to the intrinsic enhancement of the damping. The availability of $5d$ electrons in the NM layer and the opportunity for hybridization with the $3d$ electrons in the FM at the interface is a key mechanism which enhances the damping. This agrees with previous studies of FM-NM interfaces including the recent theoretical work of Barati *et al.* [1–3,11–21]. Extrinsic contributions to the damping can be attributed to two-magnon scattering, which is related to local variations linked to topological roughness, defects, and impurities at the interface. For discontinuous Pt it is suggested that variations in local electronic properties of the Pt capped and uncapped regions leads to local variation of intrinsic damping, which gives rise to extrinsic damping via two-magnon scattering. The precessional frequency dependence of the damping data (see Fig. 3) shows a linear increase in damping with the decreasing frequency for the discontinuous Pt layer, which clearly indicates that extrinsic effects are present in the system when the capping layer is discontinuous.

Following the initial rapid increase in region I, the damping reaches a broad peak in region II. From the structural analysis it is observed that the second region falls into the thickness range where a continuous Pt capping layer is just forming. Beyond this thickness a complete Pt layer is established.

In region III damping falls from its maximum and slowly stabilizes to an intermediate value with increasing Pt thickness.

The independence of the damping on applied field indicates the mechanism here is predominantly intrinsic when the Pt is continuous. The decrease in the damping from the peak primarily represents a reduction in the extrinsic contribution that largely vanishes for higher thicknesses of Pt. Further details of this mechanism in terms of the local arrangement of atoms at the interface are discussed later. It is interesting to observe that the final value of α_{eff} is larger than the uncapped ($t_{NM} = 0$) value for both Co and $Ni_{81}Fe_{19}$. The reason for this is that although at higher thicknesses of Pt the extrinsic contribution is negligible, intrinsic effects from the interface are the dominant contribution to the damping. Theoretical analysis [3] shows some reduction in the intrinsic damping from the peak, along with periodic oscillations due to the formation of quantum well states. Oscillations are not observed in the experiment as the t_{NM} range is too small, but also any oscillations would be lost due to interfacial roughness.

Regarding the mechanism for extrinsic damping, it is suggested that two-magnon scattering is a result of local variation of d-d hybridization of the Co and Pt when the capping layer is discontinuous, leading to localized variations of the intrinsic damping. The miscibility of the NM material changes the local structure. In the case of Pt this can produce Co-Pt clusters or islands at the surface [22], while for Au this leads to the formation of Au islands on Co in the low-thickness regime [31]. For thin Pt, where the capping layer is incomplete, the formation of clusters or islands at the surface acts to break the translational symmetry leading to regions with higher and lower intrinsic damping due to the distribution of Co-Pt. This is also supported by a study which showed that SOC for Pt is stronger when it is 2D rather than 3D, which increases the local damping of the Co-Pt islands [37]. This inhomogeneous magnetic surface can, therefore, give rise to an extrinsic contribution to the enhancement of the damping. When the Pt capping layer completely covers the Co the interface region is more uniform and the extrinsic contribution vanishes [2,3,12,18].

It is worth noting that the experimental data [Fig. 2(b)] for the precessional frequency and the saturation magnetization, M_S, of the Co/Pt system shows an increase in the net magnetic moment as the Pt capping increases. This may be attributed to a proximity induced magnetization (PIM) in Pt [12]. The role of PIM in damping remains a matter of debate [19]. Also, it can be seen that M_S for the uncapped Co is lower than expected for bulk Co, which may be related to oxidation of the uncapped Co surface. This is supported by the significant increase in M_S when t_{Pt} reaches 0.6 nm where the Pt cap would restrict the oxidation of the Co surface. However, PIM cannot explain the large addition M_S when t_{Pt} reaches to 2 nm except the case when Co/Pt thin film have hcp crystal structure, which agrees with XRD in of this study and also with the recent published research [15].

Comparing the Pt and the Au layers, greater miscibility of Pt is an additional factor affecting the damping and is supported by the XRR structural analysis [31]. As a result, two-magnon scattering is also lower in case of Co/Au. Furthermore, Au has a lower density of electrons in d band states at the Fermi level compared to Pt [38], which therefore contributes very weakly to the intrinsic damping. For $Ni_{81}Fe_{19}$/Pt the capping layer thickness dependence of the damping shows similar behavior
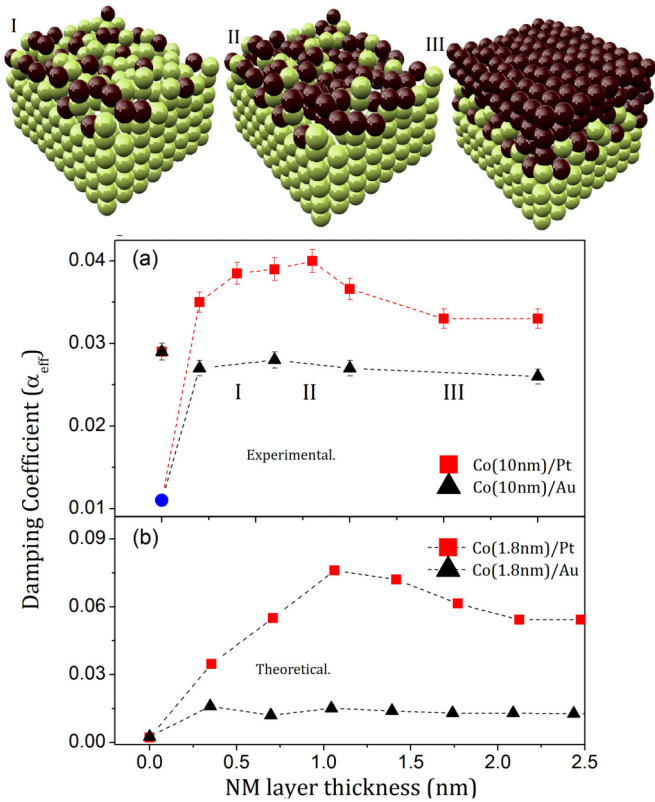
FIG. 4. Schematic illustration of the growth of discontinuous to continuous NM capping layer. (a) Experimental damping data for Co/Pt and Co/Au as a function of t_{NM}. The circular point is a literature value for pure cobalt. (b) Theoretical variation in damping data for Co/Pt and Co/Au adapted from Ref. [3] as a function of t_{NM}.

to Co/Pt. However, it can be seen from Figs. 2(a) and 2(c) that α_{eff} for $Ni_{81}Fe_{19}/Pt$ is higher at lower Pt thickness. This may be related to a slightly larger topological roughness and different FM crystal structure, as shown by the structural analysis. The larger enhancement of the damping for the $Ni_{81}Fe_{19}$, as compared to Co, may be explained by a higher spin-mixing conductance across the interface for fcc rather than hcp FM interfacial structure [15,39]. This is supported by the experimental XRD results showing hcp Co and fcc $Ni_{81}Fe_{19}$ in the FM/NM bilayers.

Bringing together the structural analysis and the discussion of the damping mechanisms the interpretation of the NM capping layer thickness dependence of the ferromagnetic damping is summarized in Fig. 4, where the structural changes associated with the thickness dependence of the damping are illustrated for regions, I, II, and III.

Figure 4 also shows a comparison between the experimental damping data and the theoretical analysis of Co/Pt and Co/Au by Barati *et al.* [3]. The general trends of rapidly increasing damping to a peak followed by a small reduction and then leveling out of the damping with increasing film thickness are broadly similar between the theory and experiment results. Figure 4(b) shows some reduction in the intrinsic damping from the peak. In Fig. 4(a) oscillations are not observed as the t_{NM} range is too small, but overall there is good agreement between the Barati *et al.* study and this work.

Finally, the spin-mixing conductance has been estimated for both Co/Pt and $Ni_{81}Fe_{19}/Pt$ from the damping data obtained for samples with the thickest Pt layer, where the Pt has formed a complete capping layer and measurements indicate that the mechanism for the enhanced damping is intrinsic. The spin-mixing conductance is related to the change in damping according to:

$$\Delta \alpha = \alpha_{eff} - \alpha_0 = \frac{g \mu_B}{4 \pi M_{eff} t_{FM}} g_{\uparrow\downarrow}^{eff}, \tag{3}$$

where g is the Landé g factor, μ_B is the Bohr magneton, M_{eff} is the effective saturation magnetization, and $g_{\uparrow\downarrow}^{eff}$ is the effective spin-mixing conductance.

Taking literature values for the damping in bulk hcp Co as 0.011 [21] and fcc $Ni_{81}Fe_{19}$ as 0.010 [30] and saturation magnetization as obtained experimentally, the effective spin-mixing conductance was estimated from the observed saturation enhancement to the damping. For Co/Pt a value of 38 nm^{-2} was obtained for the spin-mixing conductance, which is comparable with the value recently observed experimentally [19]. In the case of $Ni_{81}Fe_{19}/Pt$ a value of 125 nm^{-2} was obtained. This is notably higher than the value obtained for Co/Pt and it is suggested that this may be related to the different crystallographic structures at the interface with the Pt. This is supported by recent work on Co/Ir where the Co structure at the interface was either hcp or fcc [15].

VI. CONCLUSIONS

In conclusion, precessional magnetization damping has been studied in different FM/NM bilayer thin films with a gradually increasing capping layer thickness starting from the sub-monolayer regime. For Pt capping of Co and $Ni_{81}Fe_{19}$ the Pt thickness-dependent damping shows an increase followed by a peak and a modest fall to constant value that is higher than the bulk values for Co and $Ni_{81}Fe_{19}$. Structural analysis using x-ray reflectivity and x-ray diffraction were used to characterize the interface and the crystallographic structure and aid the interpretation. Both intrinsic and extrinsic mechanisms are invoked to explain the observed magnetic precessional damping behavior. Extrinsic effect occurs when the Pt capping layer is incomplete as it leads to variation in d-d hybridization leading to inhomogeneities in damping which can act to create two-magnon scattering. This extrinsic damping is lost when the Pt layer became continuous over the FM. Finally the effective spin-mixing conductance was estimated for $Ni_{81}Fe_{19}/Pt$ and Co/Pt. The analysis indicates that the effective spin-mixing conductance is higher in $Ni_{81}Fe_{19}/Pt$ than Co/Pt and it is suggested that this may be linked to the crystal structure type and the interface properties. The results provide further insight into the mechanism of damping variation in FM/NM bilayer when the interfacial region is gradually formed.

---

[1] K. Lenz, H. Wende, W. Kuch, K. Baberschke, K. Nagy, and A. Jánossy, Phys. Rev. B **73**, 144424 (2006).

[2] J. Rantschler, R. McMichael, A. Castillo, A. Shapiro, W. Egelhoff, B. Maranville, D. Pulugurtha, A. Chen, and L. Connors, J. Appl. Phys. **101**, 033911 (2007).

[3] E. Barati, M. Cinal, D. M. Edwards, and A. Umerski, Phys. Rev. B **90**, 014420 (2014); EPJ Web Conf. **40**, 18003 (2013).

[4] A. Ganguly, S. Azzawi, S. Saha, J. King, R. Rowan-Robinson, A. Hindmarch, J. Sinha, D. Atkinson, and A. Barman, Sci. Rep. **5**, 17596 (2015).

[5] Y. Tserkovnyak, A. Brataas, and G. E. W. Bauer, Phys. Rev. Lett. **88**, 117601 (2002).

[6] K. Chen and S. Zhang, Phys. Rev. Lett. **114**, 126602 (2015).

[7] G. Woltersdorf, M. Buess, B. Heinrich, and C. H. Back, Phys. Rev. Lett. **95**, 037401 (2005).

[8] Y. Liu, Z. Yuan, R. J. H. Wesselink, A. A. Starikov, and P. J. Kelly, Phys. Rev. Lett. **113**, 207202 (2014).

[9] G. Malinowski, F. Dalla Longa, J. Rietjens, P. Paluskar, R. Huijink, H. Swagten, and B. Koopmans, Nat. Phys. **4**, 855 (2008).

[10] G. Zhang, W. Hübner, G. Lefkidis, Y. Bai, and T. F. George, Nat. Phys. **5**, 499 (2009).

[11] K. Kyuno, J.-G. Ha, R. Yamamoto, and S. Asano, Phys. Rev. B **54**, 1092 (1996).

[12] Y. Sun, H. Chang, M. Kabatek, Y.-Y. Song, Z. Wang, M. Jantz, W. Schneider, M. Wu, E. Montoya, B. Kardasz *et al.*, Phys. Rev. Lett. **111**, 106601 (2013).

[13] N. Nakajima, T. Koide, T. Shidara, H. Miyauchi, H. Fukutani, A. Fujimori, K. Iio, T. Katayama, M. Nývlt, and Y. Suzuki, Phys. Rev. Lett. **81**, 5229 (1998).

[14] R. Urban, G. Woltersdorf, and B. Heinrich, Phys. Rev. Lett. **87**, 217204 (2001).

[15] M. Tokaç, S. A. Bunyaev, G. N. Kakazei, D. S. Schmool, D. Atkinson, and A. T. Hindmarch, Phys. Rev. Lett. **115**, 056601 (2015).

[16] S. Iihama, S. Mizukami, H. Naganuma, M. Oogane, Y. Ando, and T. Miyazaki, Phys. Rev. B **89**, 174416 (2014).

[17] A. Barman, S. Wang, O. Hellwig, A. Berger, E. E. Fullerton, and H. Schmidt, J. Appl. Phys. **101**, 09D102 (2007).

[18] M. C. Hickey and J. S. Moodera, Phys. Rev. Lett. **102**, 137601 (2009).

[19] J.-C. Rojas-Sánchez, N. Reyren, P. Laczkowski, W. Savero, J.-P. Attané, C. Deranlot, M. Jamet, J.-M. George, L. Vila, and H. Jaffrès, Phys. Rev. Lett. **112**, 106602 (2014).

[20] S. Mizukami, E. Sajitha, D. Watanabe, F. Wu, T. Miyazaki, H. Naganuma, M. Oogane, and Y. Ando, Appl. Phys. Lett. **96**, 152502 (2010).

[21] S. Pal, B. Rana, O. Hellwig, T. Thomson, and A. Barman, Appl. Phys. Lett. **98**, 082501 (2011).

[22] T. Blon, G. B. Assayag, J.-C. Ousset, B. Pecassou, A. Claverie, and E. Snoeck, Nucl. Instrum. Methods B **257**, 374 (2007).

[23] J. A. King, A. Ganguly, D. Burn, S. Pal, E. Sallabank, T. Hase, A. Hindmarch, A. Barman, and D. Atkinson, Appl. Phys. Lett. **104**, 242410 (2014).

[24] T. L. Gilbert, IEEE Trans. Magn. **40**, 3443 (2004).

[25] R. Conger and G. Moore, J. Appl. Phys. **34**, 1213 (1963).

[26] P. S. Keatley, V. Kruglyak, P. Gangmei, and R. Hicken, Philos. Trans. R. Soc. Lond. A **369**, 3115 (2011).

[27] A. Barman and A. Haldar, *Solid State Physics*, Vol. 65, edited by R. E. Camley and R. L. Stamps (Academic Press, San Diego, CA, 2014), p. 1.

[28] D. K. Bowen and B. K. Tanner, *High Resolution X-ray Diffractometry and Topography* (CRC Press, Boca Raton, FL, 2005); *X-ray Metrology in Semiconductor Manufacturing* (CRC Press, Boca Raton, FL, 2006).

[29] M. Björck and G. Andersson, J. Appl. Crystallogr. **40**, 1174 (2007).

[30] L. G. Parratt, Phys. Rev. **95**, 359 (1954).

[31] H. Baker, ASM Handbook, Vol. 3: Alloy Phase Diagrams, edited by H. Baker, Materials Park, OH: ASM International, 1992 (1992), pp. 1.1–1.29.

[32] A. Umerski (personal communication).

[33] S. Mizukami, Y. Ando, and T. Miyazaki, Phys. Rev. B **66**, 104413 (2002).

[34] S. Mizukami, Y. Ando, and T. Miyazaki, J. Magn. Magn. Mater. **239**, 42 (2002).

[35] A. Ruiz-Calaforra, T. Brächer, V. Lauer, P. Pirro, B. Heinz, M. Geilen, A. Chumak, A. Conca, B. Leven, and B. Hillebrands, J. Appl. Phys. **117**, 163901 (2015).

[36] R. M. Rowan-Robinson, A. T. Hindmarch, and D. Atkinson, (unpublished).

[37] M. N. Huda, M. K. Niranjan, B. R. Sahu, and L. Kleinman, Phys. Rev. A **73**, 053201 (2006).

[38] C. Fadley and D. Shirley, J. Res. Natl. Bur. Stand. A **74A**, 543 (1970).

[39] J. Huang, T. Wang, C. Yu, Y. Hu, P. Lee, and M. Yang, J. Cryst. Growth **171**, 442 (1997).